

Surface Chemistry

Terminal Alkyne Coupling on a Corrugated Noble Metal Surface: From Controlled Precursor Alignment to Selective Reactions

Tao Lin,^[a] Liding Zhang,^[a] Jonas Björk,^[b] Zhi Chen,^[c] Mario Ruben,^[c, d] Johannes V. Barth,^[a] and Florian Klappenberger*^[a]

Abstract: Surface-templated covalent coupling of organic precursors currently emerges as a promising route to the atom-precise fabrication of low-dimensional carbon materials. Here, we investigate the adsorption and the coupling reactions of 4,4''-diethynyl-1,1':4',1''-terphenyl on Au(110) under ultra-high vacuum conditions by using scanning tunneling microscopy combined with density functional theory and kinetic Monte Carlo calculations. Temperature treatment induces both 1,2,4-asymmetric cyclotrimerization and homocoupling, resulting in various reaction products, including a previously unreported, surface-templated H-shaped pentamer. Our analysis of the temperature-dependent relative product abundances unravels that 1,2,4-trimerization and homocoupling proceed via identical intermediate species with the final products depending on the competition of coupling to a third monomer versus dehydrogenation. Our study sheds light on the control of coupling reactions by corrugated surfaces and annealing protocols.

On-surface synthesis via covalent coupling of molecular precursors represents a promising route toward the fabrication of functional nanomaterials with applications in molecular electronics, sensors, catalysis, and optoelectronic devices.^[1] The atomistic real-space visualization of scanning probe microscopy offers comprehensive insights into the involved reactions by resolving reactants, intermediates, and products down to the sub-molecular level.^[2]

Nowadays, numerous promising reactions have been identified for the bottom-up construction of covalent nanoarchitectures, including Ullmann coupling,^[3] condensation reactions,^[4] and azide-alkyne cycloaddition.^[5] Coupling of terminal alkynes appears as a specifically prosperous approach because of (quasi) byproduct-free reactions, namely cyclotrimerization (including asymmetric 1,2,4- and symmetric 1,3,5-cyclotrimerization) and homocoupling.^[6] It has been demonstrated that thermal activation can trigger both reactions on various flat metal surfaces (i.e., Au, Ag, Cu), whereby a preference for cyclotrimerization and homocoupling is expressed on Au(111) and Ag(111), respectively. As a drawback, their complex, multistep pathways^[6e,7] render these reactions prone to a variety of side-reactions,^[8] thus achieving selective alkyne coupling remains challenging.

Carrying out synthesis on a surface opens up innovative methods to control the involved elementary reactions. For example, embedding alkane chains in the grooves of the reconstructed Au(110) surface enabled their otherwise challenging linear polymerization.^[9] Enforcing parallel alignment of their building blocks by step-edge attachment on a vicinal surface afforded the first graphdiyne-related semiconducting molecular wires.^[6f] On the other hand, controlling key factors such as reaction kinetics and energetics through different annealing procedures allowed to deliberately select intermolecular versus intramolecular reactions of a multitopic monomer.^[10]

Here, we explore the influence of the highly corrugated and anisotropic Au(110) surface on the coupling reactions of a terminal alkyne compound with respect to achieving well-defined nanoscaffolds. More specifically, we investigate the adsorption configurations and covalent transformations of 4,4''-diethynyl-1,1':4',1''-terphenyl molecules (DETP, shown in Figure 1a) using scanning tunneling microscopy (STM) (performed at 5.5 K) combined with density functional theory (DFT) and kinetic Monte Carlo (kMC) calculations. The distinct adsorption configurations on the Au(110) surface allow us to classify products formed through alkyne cyclotrimerization and homocoupling. We demonstrate that the surface templating effect decisively influences the product formation, affording, amongst other scaffolds, an H-shaped pentamer previously inaccessible through solution chemistry. Furthermore, by establishing a relation between reaction conditions and obtained products, our work delivers a guideline for increasing chemoselectivity.

To identify the favorable adsorption site of DETP, a small concentration of molecules ($\approx 0.17 \text{ nm}^{-2}$) was deposited onto the Au(110) substrate, which was held at 200 K. As shown in

[a] Dr. T. Lin, L. Zhang, Prof. Dr. J. V. Barth, Prof. Dr. F. Klappenberger
Physik-Department E20
Technische Universität München
James-Franck-Str., 85748 Garching (Germany)
E-mail: florian.klappenberger@tum.de

[b] Prof. Dr. J. Björk
Department of Physics, Chemistry, and Biology (IFM), Linköping University,
58183 Linköping (Sweden)

[c] Dr. Z. Chen, Prof. Dr. M. Ruben
Institute of Nanotechnology
Karlsruhe Institute of Technology
76344 Eggenstein-Leopoldshafen (Germany)

[d] Prof. Dr. M. Ruben
IPCMS-CNRS University de Strasbourg
23 Rue de Loess, 67034 Strasbourg (France)

Supporting information and the ORCID identification number(s) for the author(s) of this article can be found under <https://doi.org/10.1002/chem.201701735>.

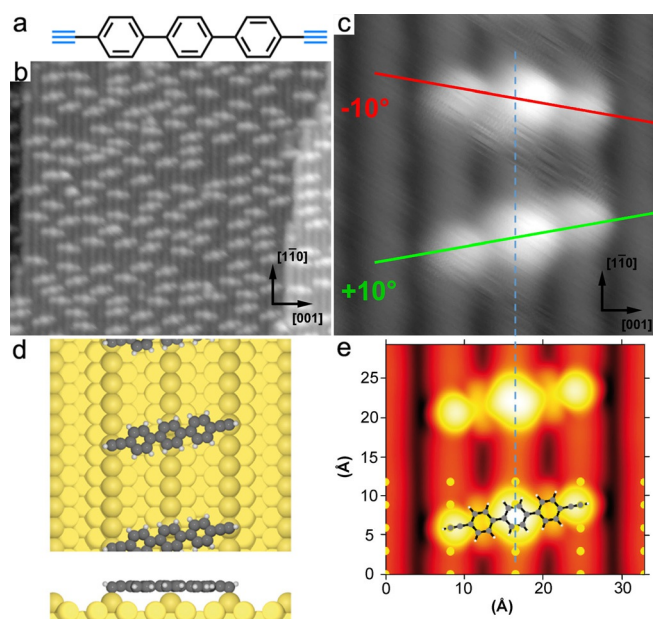


Figure 1. a) Chemical structure of DETP (4,4''-diethynyl-1,1':4',1''-terphenyl). b) STM image ($32 \times 27 \text{ nm}^2$) of DETP molecules distributed on Au(110). c) Close-up STM image ($4 \times 4 \text{ nm}^2$) showing two DETP molecules with different orientations indicated by the green and red lines, respectively. d) The energetically favored adsorption geometry obtained from DFT calculations. e) Simulated STM image ($U = -1 \text{ V}$) of two molecules, one with superposed molecular structures and gold atom positions (yellow dots). The blue dashed line indicates the central gold atom row.

Figure 1b, DETP molecules are almost uniformly distributed on the surface and an individual entity appears as a rod with a central bright protrusion and two slightly dimmer dots at both sides. A single molecule exhibits an orientation that is almost perpendicular to the $[1\bar{1}0]$ direction of the surface exhibiting the 1×2 missing row reconstruction. In a close-up STM image (Figure 1c), two isolated molecules with two different orientations (green and red lines) can be observed; their main axes are oriented $\pm 10^\circ$ to the $[001]$ direction, respectively.

For a better understanding of the surface bonding, systematic DFT calculations were carried out. In total, we considered eight different adsorption configurations, featuring different alignment and epitaxy with the substrate (Figure S1 in the Supporting Information). The energetically preferred configuration is depicted in Figure 1d. The epitaxy is given by the alkyne groups being anchored to top sites of the protruding atomic rows and the central phenyl ring residing over a bridge site. Such anchoring induces a main axis deviation of 10.2° from the $[001]$ direction, which agrees well with the experimental results. Moreover, the simulated STM image of this configuration (Figure 1e) displays a central bright protrusion with neighboring slightly dimmer features. The pronounced agreement with the experimental contrast (cf. Figure 1c) confirms the proposed adsorption configuration. The observation of a closely related adsorption mode for a three-fold symmetric alkyne derivative (see the Supporting Information, Figure S2) suggests that such alkyne anchoring is generally decisive for the epitaxy of hydrocarbon precursors containing C–C triple bonds.

Covalent coupling reactions between the terminal alkyne groups were induced by annealing the sample at $T_{\text{ann}} = 340 \text{ K}$ for 10 min. As shown in Figure 2a, besides isolated monomers, novel species can be identified on the surface; tree-fork-shaped trimers, H-shaped pentamers, and linear dimers are marked in red, green, and orange ellipses, respectively. The close-up STM images given in Figures 2b–d summarize these typical covalent products (other rare products are shown in Figure S3 in the Supporting Information) and the abundance ratio among these structures is 1:0.23:0.26.

The trimer (Figure 2b) shows a tree-fork shape with angles of 60° , 120° , and 180° between coupled units, which indicates that an asymmetric 1,2,4-trisubstituted benzene ring was produced through cyclotrimerization. To further confirm that the tree-fork species (Figure 2b) results from a cyclotrimerization, rather than from a potential side reaction as identified beforehand,^[8] DFT calculations were carried out. As shown in Figure S4 in the Supporting Information, we considered two kinds of trimers through 1,2,4-cyclotrimerization and a side reaction. From STM experiments (Figure 2e), it is found that the longer branch of this trimer is slightly bent, rather than straight. Moreover, a closer inspection reveals that the trimer displays intra-

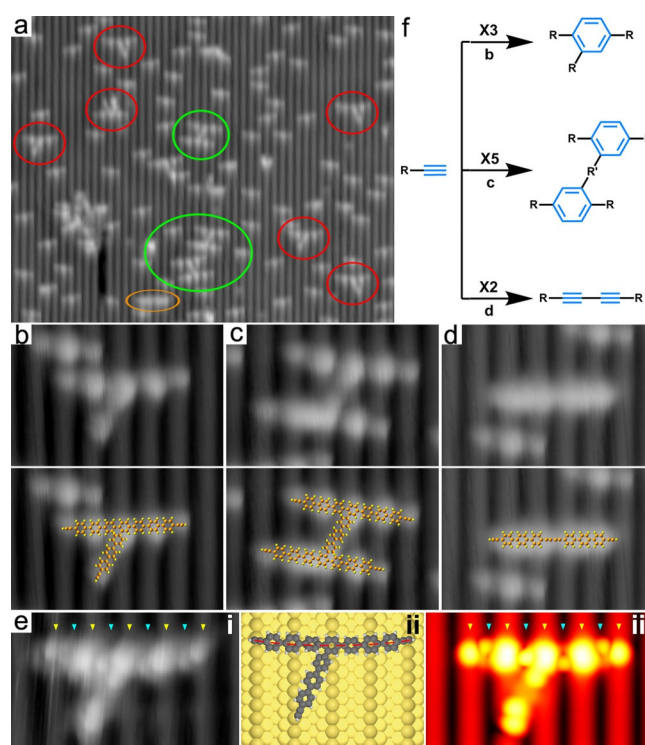


Figure 2. a) STM image ($40 \times 32 \text{ nm}^2$) after 340 K annealing. The different coupling products, trimers, pentamers, and dimers, are marked by red, green, and orange ellipses, respectively. b–d) Close-up STM images (all $6 \times 4 \text{ nm}^2$) of a trimer, pentamer, and dimer; lower row superposed with simplified models. e) Close-up STM image ($5 \times 3 \text{ nm}^2$); i) the energetically favored adsorption geometry, ii) and the simulated STM image ($U = -1 \text{ V}$) iii) of a tree-fork-shaped trimer. The cyan and yellow triangles point to the main and satellite dots, respectively. The red dashed line indicates the curved feature of the trimer. f) Scheme of the conversion of monomers to the suggested coupling products. R and R' are the rest parts of the molecule and the terphenyl backbone, respectively.

molecular corrugation features along the longer side, i.e., five main bright dots and four satellite dots, marked by the cyan and yellow triangles, respectively. Figure 2eii shows the energetically favored adsorption configuration of the cyclotrimerized trimer from the DFT calculations. The longer branch exhibits a curved geometry, which results from the central phenyl ring residing over a bridge site and the terminal alkyne groups being anchored to top sites. Furthermore, the corresponding simulated STM image (Figure 2eiii) displays features of main and satellite dots in nice agreement with the experiment. The main protrusions are evoked from phenylene rings residing on top of atomic rows. The satellite lobes are related to the tilted rings positioned over the reconstruction grooves (Figure S4b in the Supporting Information). In contrast, the simulated results of the trimer generated by alkyne cross-coupling (Figure S4d) disagree in curvature of the longer branch and the positioning of the satellite features next to the trimerized moiety. Therefore, the cross-coupled species can be safely ruled out, corroborating our assignment in Figure 2 f.

In previous work, it has been demonstrated that both symmetric 1,3,5-trisubstituted and asymmetric 1,2,4-trisubstituted benzene rings can be formed from 4,4'-diethynyl-1,1'-biphenyl on Au(111), whereby the intrinsic reasons why one or the other occurs remained unaddressed.^[6e] In our case, the symmetric product (cf. Figure S3 in the Supporting Information) is very scarce, occurring only in approximately 1 out of 150 cases of all trimer connections, revealing that the anisotropic reconstruction pattern plays a key role in the formation of the asymmetric trimers and in the suppression of the symmetric products.

The close-up STM images of an H-shaped pentamer and the corresponding simplified structural model are shown in Figure 2c. The larger scaffold expresses similar contrast features of the trimer asymmetric indicating that the H-shaped pentamer contains two asymmetric 1,2,4-trisubstituted benzene rings formed through cyclotrimerization. Note that the angles between coupled units in an asymmetric benzene ring in this species are 70°, 110°, and 180°, probably due to the highly site-selective interaction between the pentamer and the substrate.

Besides the cyclotrimerization products, linear oligomers formed through homocoupling can also be observed and the representative STM image of a straight dimer is depicted in Figure 2d. Unlike the single monomers deviating by $\pm 10^\circ$, the dimers are parallel with the [001] direction within the experimental resolution. The appearance of the dimer does not display the clear intramolecular features of previous species. The more uniform brightness allows distinguishing the homocoupled products from those of cyclotrimerization. The dimer alignment perpendicular to the surface grooves is in marked contrast to previous results in which linear polymerization has been achieved within adsorption-induced (1×3) reconstruction grooves of Au(110).^[9,11] The difference is ascribed to the alkyne-mediated molecule–surface interactions that enforce specific adsorption configurations of the DETP precursors and linear wire segments.

For comparison, we prepared a sample that we directly annealed at 400 K after deposition of the molecules. Representative STM images are shown in Figure 3a. From the above discussion, the intramolecular corrugation features can be used to distinguish the cyclotrimerized and homocoupled products. Accordingly, the data in Figure 3a evidences the increased abundance of linear oligomers. During the temperature treatment, the molecular coverage decreased significantly, indicating that desorption interferes at 400 K.

A third sample was produced in which molecules were deposited onto the substrate held at 460 K (Figure 3b). Again, linear oligomers prevail, while only a minority of cyclotrimerized species is present. A comparison of the length distributions of the latter two samples is provided in Figure 3c and reveals that the fraction of longer oligomers is larger for the hot deposition at 460 K, indicating that such conditions are beneficial for fabricating molecular wires.

The statistical analysis of the relative product abundance observed on these samples is depicted in Figure 3d. Note that the category “other” includes all minority species the chemical nature of which could not be conclusively disentangled. They result from side reactions,^[8] spurious effects related to impurities originating from the substrate, or impurities in the starting compound used for evaporation. Accordingly, the number of molecules involved in “other” is an estimation based on the

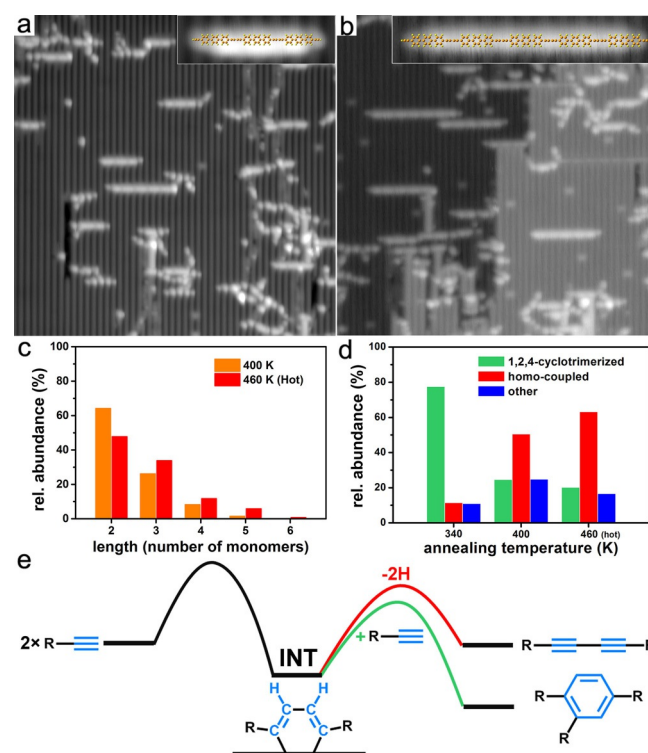


Figure 3. a) STM image ($40 \times 40 \text{ nm}^2$) after standard 400 K annealing. Inset: a linear trimer. b) STM image ($40 \times 40 \text{ nm}^2$) after hot deposition with the substrate held at 460 K. Inset: a linear pentamer. c) Relative product abundances for different annealing recipes. d) The oligomer length distribution of the sample after 400 K annealing and hot deposition with the substrate held at 460 K, respectively. e) A simplified reaction scheme illustrating the unified coupling scenario including homocoupling and asymmetric cyclotrimerization.

apparent cluster size as imaged by STM (see explanation in Methods in the Supporting Information). Moreover, the varying preparation parameter for the annealing or hot deposition treatments imply markedly different rates for desorption of monomers, for which the given percentages do not represent reaction yields. For $T_{\text{ann}} = 340$ K, 1,2,4-cyclotrimerization products prevail on the sample and the occurrence ratio of linkages via cyclotrimerization and homocoupling is approximately 8:1. The dominance of trimerization is indicative of a lower activation energy compared to homocoupling. Noteworthy, the temperature for cyclotrimerization on Au(110) is lower than that on Au(111), for which 373 K are required.^[6d,e] We attribute this to an increased catalytic activity due to the corrugation of the (110) surface, resulting in a lower coordination of its surface atoms. For the other two samples, the pertaining relative abundances reproduced in Figure 3d give a ratio of 1:2 and 1:3, clearly indicating that the system prefers homocoupling over cyclotrimerization at higher T_{ann} .

In a classical pathway picture of two competing reactions with differently high barriers and under thermodynamic conditions, the reaction with the higher barrier can never be favored, even for high temperatures. Thus, the explanation of the observed temperature dependence of the prevailing reactions requires a more complex scenario. For its discussion (Figure 3e), we simplify the proposed pathway for homocoupling^[7] to two major steps: 1) Two pristine molecules couple to an intermediate (INT), which is bound to the substrate and has two hydrogen atoms pointing away from the substrate; 2) The INT finalizes the homocoupling by two subsequent dehydrogenation steps. Previous results indicate that cyclotrimerization also proceeds via a two-step reaction with essentially the same INT.^[6e] The second step of the cyclotrimerization is an intermolecular reaction depending on the kinetic supply of a third monomer by diffusion and can only occur as long as the hydrogens have not been abstracted. From theoretical results^[6b,e,7] it is clear that cyclotrimerization is the more exothermic reaction. The thus constructed unified reaction Scheme (Figure 3e) explains several observations. First, the surface-templated positioning of monomers triggers the formation of an INT having residual (R) groups connected at 1,4 positions. Then at lower T_{ann} (340 K) cyclotrimerization takes place more frequently than homocoupling due to both its lower reaction barrier and the fact that the hydrogen abstraction rate is obviously slower than the supply of reactants. In contrast, at higher T_{ann} (e.g., 400 K), the dehydrogenation of the INT proceeds faster than the supply of reactants, rendering homocoupling more probable than cyclotrimerization, despite having a higher energy barrier. Additionally, above 400 K, cyclotrimerization is further suppressed by desorption of DETP monomers. In sum, the competition between the connection of a third monomer to the INT and the dehydrogenation of the INT gives the thermal selectivity toward different reaction products. Similar observations have recently been reported for intermolecular and intramolecular reactions, in which a low-barrier intermolecular reaction was observed at moderate temperatures, while a high-barrier intramolecular reaction was observed at higher temperatures.^[10]

To corroborate our hypothesized reaction scenario, we used kMC simulations^[3e,12] to model the reactions of DETP according to our unified reaction Scheme (cf. Figure 3e). For the barriers of the black, green, and red path, we chose 0.9 eV,^[7] 0.8 eV, and 0.95 eV, respectively. Details of the kMC simulation algorithm can be found in the Supporting Information. Figure 4a,b

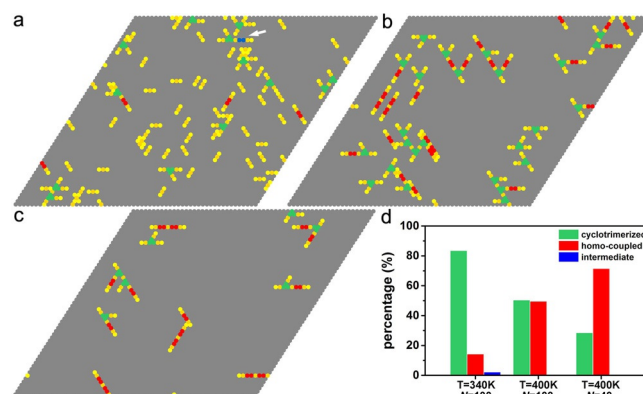


Figure 4. a–c) kMC (kinetic Monte Carlo) simulated structures formed at different total number of molecules (N) and temperatures: a) $N = 100$ at 340 K, b) $N = 100$ at 400 K, and c) $N = 40$ at 400 K. The white arrow in (a) indicates an INT (intermediate). d) Statistical results of different kMC samples.

show the simulated structures with the identical total number of molecules ($N = 100$, which corresponds to about 0.08 ML; 1 ML corresponds to a close-packed structure that have all sites occupied) at 340 K and 400 K, respectively. At 340 K, most reaction products result from cyclotrimerization, while as the temperature rises, the portion of homocoupled connections increases. From the statistical results (Figure 4d), the ratio between cyclotrimerized and homocoupled products changes from about 6:1 to 1:1 upon increase of temperature. To further promote homocoupled bonds, we considered the fact that desorption starts to occur at 400 K. Thus, we decreased N to 40 and the corresponding simulated structure is shown in Figure 4c. The corresponding ratio is about 1:2.5, close to our experimental findings. Although the energy barrier values may not fully agree with the experimental ones and some features such as the corrugated substrate, heating and cooling processes are not taken into account, the kMC simulations qualitatively support the proposed model of reaction pathways.

For two-step sequential reactions with an intermediate state representing a local energy minimum, it is expected that trapped species resulting from incomplete reactions should exist. Indeed, such intermediates occur in the simulations (cf. Figure 4a, blue species, highlighted by arrow). However, they are rare and have only been observed for the milder annealing treatment. Also in the experiment, some species are discernible (see Figure S5 in the Supporting Information), which occur similarly infrequent and are tentatively attributed to trapped intermediates.

Our own findings and those of previous studies of on-surface and solution polymerization^[13] of alkynes allow us to understand the surface influence on the coupling process

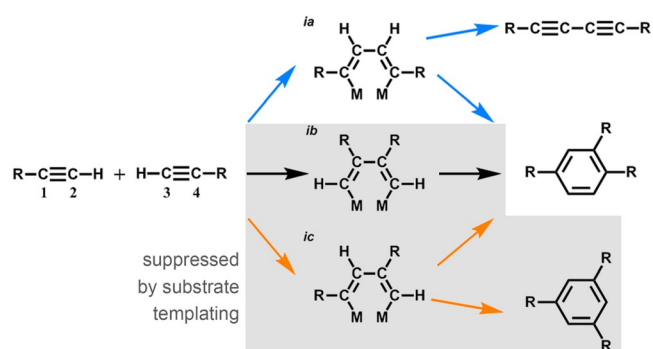


Figure 5. A reaction scheme illustrating the alkyne coupling pathways leading to homocoupling and cyclotrimerization through the various possible intermediates. Pathways suppressed by the substrate templating effect are marked by the gray background.

(Figure 5). Noteworthy, this analysis bases exclusively on the clearly identified reaction products, thus the conclusions are unaltered by the presence of unidentified minority species. In this picture, we consider that R-groups are attached to 1,4 carbons and that the two pristine alkynes initially couple into one out of three INTs; *ia* (coupling between two outermost carbons, initially 2,3), *ib* (coupling between two penultimate carbons, initially 1,4), and *ic* (coupling between an outermost and a penultimate carbon, initially 1,3 or 2,4). All three INTs can yield 1,2,4-cyclotrimerized products. Dehydrogenation of *ia* forms the homocoupled product. The addition of a third alkyne to *ic* in the right orientation leads to 1,3,5-cyclotrimerized products. From previous reports, the involvement of the INTs *ia* and *ic* in surface-confined reactions is evident, since they are compulsory for homocoupling and 1,3,5-cyclotrimerization, respectively. However, there is no evidence for the INT *ib*, which should be considered as a hypothetical INT to be verified or refuted by later studies. With this picture, it is possible to explain the diversity of the reactions occurring under various conditions, i.e., for different precursor/substrate combinations. On the flat Ag(111) surface and with the right choice of precursors,^[6a,c] the barriers for *ia* and subsequent H abstraction can be small enough such that the reaction proceeds via *ia* and yields homocoupling with high preference. On the flat Au(111) surface, Zhou et al. reported^[6e] both 1,2,4- and 1,3,5-cyclotrimerization and discussed intermediates with straight and 120° kinked geometries, respectively. Both intermediates were assigned to *ia* isomers, which is unlikely because going from *ia* to 1,3,5 rings requires the breaking of C–R bonds. We propose instead that both *ia* and *ic* are involved in the cyclotrimerization reactions. Moreover, it was reported that by establishing a steric pre-arrangement by a high enough coverage of three-fold symmetric molecules,^[6d] 1,3,5-cyclotrimerization can be dominating. This is consistent with the suppression of INT *ia* via the geometric constraints of the dense packing. In our case, the site-specific molecule–substrate interaction templates the arrangement of the reactants such that intermediates *ib* and *ic* are suppressed and the largely dominating part of the coupling reactions proceeds via *ia* as already suggested in Figure 3e. The final outcome then depends on the relative proba-

bilities of energetically limited hydrogen abstraction and kinetically limited reactant supply.

In conclusion, we have reported unprecedented insights in controlling terminal alkyne coupling with highly corrugated surfaces. First, we demonstrated that the substrate induced a well-defined and favorable alignment of the reactive groups in which the molecular backbone is intriguingly perpendicular to the surface grooves. Such surface-induced prepositioning is expected to be fruitful also for other on-surface synthesis approaches in which the coupling is accounted for by reactions not directly linked to the alkyne moieties. Then, at lower annealing temperature, cyclotrimerization dominates, whereby the anisotropic surface triggers highly selective 1,2,4 pathways, resulting in previously unreported nanoscaffolds. The obtained understanding of the relation of different on-surface alkyne coupling pathways allows selection of linear homocoupling versus cyclotrimerization to a high degree. The achieved insights represent important progress for future optimization of alkyne coupling toward the desired ultimate selectivity required for the on-surface synthesis of atom-precise carbon-based materials beyond graphene.

Acknowledgements

M.R. would like to thank for the generous support by the DFG priority program 1459. This work is also supported by the European Union via ERC Advanced Grant MolArt (no. 247299) and China Scholarship Council (Z.C.). L.Z. thanks the IMPRS-APS for a scholarship. T.L. thanks the TUM University Foundation for a postdoctoral fellowship.

Conflict of interest

The authors declare no conflict of interest.

Keywords: corrugated surface · covalent coupling · scanning tunneling microscopy · surface chemistry · terminal alkyne

- [1] a) A. Gourdon, *Angew. Chem. Int. Ed.* **2008**, *47*, 6950–6953; *Angew. Chem.* **2008**, *120*, 7056–7059; b) D. F. Perepichka, F. Rosei, *Science* **2009**, *323*, 216–217; c) G. Franc, A. Gourdon, *Phys. Chem. Chem. Phys.* **2011**, *13*, 14283–14292; d) J. W. Colson, W. R. Dichtel, *Nat. Chem.* **2013**, *5*, 453–465; e) X.-H. Liu, C.-Z. Guan, D. Wang, L.-J. Wan, *Adv. Mater.* **2014**, *26*, 6912–6920; f) X. Zhuang, Y. Mai, D. Wu, F. Zhang, X. Feng, *Adv. Mater.* **2015**, *27*, 403–427.
- [2] a) M. Lackinger, W. M. Heckl, *J. Phys. D* **2011**, *44*, 464011; b) M. El Garah, J. M. MacLeod, F. Rosei, *Surf. Sci.* **2013**, *613*, 6–14; c) L. Dong, P. N. Liu, N. Lin, *Acc. Chem. Res.* **2015**, *48*, 2765–2774; d) Q. Fan, J. M. Gottfried, J. Zhu, *Acc. Chem. Res.* **2015**, *48*, 2484–2494; e) F. Klappenberger, Y.-Q. Zhang, J. Björk, S. Klyatskaya, M. Ruben, J. V. Barth, *Acc. Chem. Res.* **2015**, *48*, 2140–2150.
- [3] a) L. Grill, M. Dyer, L. Lafferentz, M. Persson, M. V. Peters, S. Hecht, *Nat. Nanotechnol.* **2007**, *2*, 687–691; b) J. Cai, P. Ruffieux, R. Jaafar, M. Bieri, T. Braun, S. Blankenburg, M. Muoth, A. P. Seitsonen, M. Saleh, X. Feng, K. Müllen, R. Fasel, *Nature* **2010**, *466*, 470–473; c) W. Wang, X. Shi, S. Wang, M. A. Van Hove, N. Lin, *J. Am. Chem. Soc.* **2011**, *133*, 13264–13267; d) L. Lafferentz, V. Eberhardt, C. Dri, C. Africh, G. Comelli, F. Esch, S. Hecht, L. Grill, *Nat. Chem.* **2012**, *4*, 215–220; e) T. Lin, X. S. Shang, J. Adisojojoso, P. N. Liu, N. Lin, *J. Am. Chem. Soc.* **2013**, *135*, 3576–3582; f) Q. Fan, C. Wang, Y. Han, J. Zhu, W. Hieringer, J. Kuttner, G. Hilt, J. M.

- Gottfried, *Angew. Chem. Int. Ed.* **2013**, *52*, 4668–4672; *Angew. Chem.* **2013**, *125*, 4766–4770; g) J. Adisoejoso, T. Lin, X. S. Shang, K. J. Shi, A. Gupta, P. N. Liu, N. Lin, *Chem. Eur. J.* **2014**, *20*, 4111–4116; h) J. Eichhorn, D. Nieckarz, O. Ochs, D. Samanta, M. Schmittel, P. J. Szabelski, M. Lackinger, *ACS Nano* **2014**, *8*, 7880–7889; i) P. Ruffieux, S. Wang, B. Yang, C. Sánchez-Sánchez, J. Liu, T. Dienel, L. Talirz, P. Shinde, C. A. Pignedoli, D. Passerone, T. Dumslaff, X. Feng, K. Müllen, R. Fasel, *Nature* **2016**, *531*, 489–492.
- [4] a) S. Weigelt, C. Busse, C. Bombis, M. M. Knudsen, K. V. Gothelf, T. Strunskus, C. Wöll, M. Dahlbom, B. Hammer, E. Lægsgaard, F. Besenbacher, T. R. Linderoth, *Angew. Chem. Int. Ed.* **2007**, *46*, 9227–9230; *Angew. Chem.* **2007**, *119*, 9387–9390; b) M. Treier, N. V. Richardson, R. Fasel, *J. Am. Chem. Soc.* **2008**, *130*, 14054–14055; c) S. Weigelt, C. Bombis, C. Busse, M. M. Knudsen, K. V. Gothelf, E. Lægsgaard, F. Besenbacher, T. R. Linderoth, *ACS Nano* **2008**, *2*, 651–660; d) S. Weigelt, C. Busse, C. Bombis, M. M. Knudsen, K. V. Gothelf, E. Lægsgaard, F. Besenbacher, T. R. Linderoth, *Angew. Chem. Int. Ed.* **2008**, *47*, 4406–4410; *Angew. Chem.* **2008**, *120*, 4478–4482; e) N. A. A. Zwaneveld, R. Pawlak, M. Abel, D. Catalin, D. Gigmes, D. Bertin, L. Porte, *J. Am. Chem. Soc.* **2008**, *130*, 6678–6679; f) J. F. Dienstmaier, D. D. Medina, M. Dogru, P. Knochel, T. Bein, W. M. Heckl, M. Lackinger, *ACS Nano* **2012**, *6*, 7234–7242; g) L. Jiang, A. C. Papageorgiou, S. C. Oh, O. Sağlam, J. Reichert, D. A. Duncan, Y.-Q. Zhang, F. Klappenberger, Y. Guo, F. Allegretti, S. More, R. Bhosale, A. Mateo-Alonso, J. V. Barth, *ACS Nano* **2016**, *10*, 1033–1041.
- [5] a) O. Díaz Arado, H. Mönig, H. Wagner, J.-H. Franke, G. Langewisch, P. A. Held, A. Studer, H. Fuchs, *ACS Nano* **2013**, *7*, 8509–8515; b) F. Bebensee, C. Bombis, S.-R. Vadapoo, J. R. Cramer, F. Besenbacher, K. V. Gothelf, T. R. Linderoth, *J. Am. Chem. Soc.* **2013**, *135*, 2136–2139.
- [6] a) Y.-Q. Zhang, N. Kepcija, M. Kleinschrodt, K. Diller, S. Fischer, A. C. Papageorgiou, F. Allegretti, J. Björk, S. Klyatskaya, F. Klappenberger, M. Ruben, J. V. Barth, *Nat. Commun.* **2012**, *3*, 1286; b) H.-Y. Gao, J.-H. Franke, H. Wagner, D. Zhong, P.-A. Held, A. Studer, H. Fuchs, *J. Phys. Chem. C* **2013**, *117*, 18595–18602; c) H.-Y. Gao, H. Wagner, D. Zhong, J.-H. Franke, A. Studer, H. Fuchs, *Angew. Chem. Int. Ed.* **2013**, *52*, 4024–4028; *Angew. Chem.* **2013**, *125*, 4116–4120; d) J. Liu, P. Ruffieux, X. L. Feng, K. Mullen, R. Fasel, *Chem. Commun.* **2014**, *50*, 11200–11203; e) H. Zhou, J. Liu, S. Du, L. Zhang, G. Li, Y. Zhang, B. Z. Tang, H.-J. Gao, *J. Am. Chem. Soc.* **2014**, *136*, 5567–5570; f) B. Cirera, Y. Q. Zhang, J. Björk, S. Klyatskaya, Z. Chen, M. Ruben, J. V. Barth, F. Klappenberger, *Nano Lett.* **2014**, *14*, 1891–1897; g) J. Liu, Q. Chen, L. Xiao, J. Shang, X. Zhou, Y. Zhang, Y. Wang, X. Shao, J. Li, W. Chen, G. Q. Xu, H. Tang, D. Zhao, K. Wu, *ACS Nano* **2015**, *9*, 6305–6314.
- [7] J. Björk, Y.-Q. Zhang, F. Klappenberger, J. V. Barth, S. Stafström, *J. Phys. Chem. C* **2014**, *118*, 3181–3187.
- [8] B. Cirera, Y.-Q. Zhang, S. Klyatskaya, M. Ruben, F. Klappenberger, J. V. Barth, *ChemCatChem* **2013**, *5*, 3281–3288.
- [9] D. Y. Zhong, J.-H. Franke, S. K. Podiyanchari, T. Blömker, H. Zhang, G. Kehr, G. Erker, H. Fuchs, L. Chi, *Science* **2011**, *334*, 213–216.
- [10] B. Cirera, N. Giménez-Agulló, J. Björk, F. Martínez-Peña, A. Martín-Jiménez, J. Rodríguez-Fernández, A. M. Pizarro, R. Otero, J. M. Gallego, P. Ballesster, J. R. Galan-Mascaros, D. Ecija, *Nat. Commun.* **2016**, *7*, 11002.
- [11] Z. Cai, L. She, L. Wu, D. Zhong, *J. Phys. Chem. C* **2016**, *120*, 6619–6624.
- [12] a) T. Lin, X. S. Shang, P. N. Liu, N. Lin, *J. Phys. Chem. C* **2013**, *117*, 23027–23033; b) Y. Li, N. Lin, *Phys. Rev. B* **2011**, *84*, 125418.
- [13] a) S. Kotha, E. Brahmachary, K. Lahiri, *Eur. J. Org. Chem.* **2005**, 4741–4767; b) J. Liu, J. W. Y. Lam, B. Z. Tang, *Chem. Rev.* **2009**, *109*, 5799–5867.

Manuscript received: April 19, 2017

Accepted manuscript online: September 8, 2017

Version of record online: October 18, 2017